The renormalization of the shell-model Gamow-Teller operator starting from effective field theory for nuclear systems

L. Coraggio,[1,2] N. Itaco,[1,2] G. De Gregorio,[1,2] A. Gargano,[2] Z. H. Cheng,[3] Y. Z. Ma,[3] F. R. Xu,[3] and M. Viviani[4]

[1]*Dipartimento di Matematica e Fisica, Università degli Studi della Campania "Luigi Vanvitelli", Viale Abramo Lincoln 5, I-81100 Caserta, Italy*

[2]*Istituto Nazionale di Fisica Nucleare, Complesso Universitario di Monte S. Angelo, Via Cintia, I-80126 Napoli, Italy*

[3]*School of Physics and Key State Laboratory of Nuclear Physics and Technology, Peking University, Beijing 100871, China*

[4]*Istituto Nazionale di Fisica Nucleare, Largo Bruno Pontecorvo 3, I-56127 Pisa, Italy*

(Received 6 July 2023; accepted 24 October 2023; published 2 January 2024)

For the first time, we approach in this work the problem of the renormalization of the Gamow-Teller decay operator for nuclear shell-model calculations by way of many-body perturbation theory, starting from a nuclear Hamiltonian and electroweak currents derived consistently by way of the chiral perturbation theory. These are the inputs we need to construct microscopically the effective shell-model Hamiltonians and decay operators. The goal is to assess the role of both electroweak currents and many-body correlations as the origins of the well-known problem of the quenching of the axial coupling constant g_A. To this end, the calculation of observables related to the Gamow-Teller transitions has been performed for several nuclear systems outside the ^{40}Ca and ^{56}Ni closed cores and compared with the available data.

DOI: 10.1103/PhysRevC.109.014301

I. INTRODUCTION

In recent years there has been a renewed interest to study the process of β decay of atomic nuclei in terms of nuclear structure theoretical models [1–13]. In fact, this kind of investigation may provide insight about the mechanism of neutrinoless double-β decay ($0\nu\beta\beta$), and also an important testing ground to validate the calculation of the nuclear matrix element $M^{0\nu}$ of such a rare decay.

An important issue which most nuclear structure calculations have to face is the overestimation of the Gamow-Teller (GT) transition rates, and this defect is usually treated by quenching the axial coupling constant g_A by a factor $q < 1$ [9,14–17]. The need to introduce effective values of g_A in nuclear structure calculations traces back to two main sources:

(1) Nucleons are not pointlike particles, and their quark structure needs to be accounted for; namely the effects of meson-exchange currents (two-body electroweak currents) have to be considered [18].
(2) Apart from the *ab initio* approaches, all other nuclear models adopt a truncation of the full Hilbert space of the configurations of the nuclear wave functions into a reduced model space where a selected number of the degrees of freedom are retained. This operation is necessary to allow the diagonalization of the nuclear Hamiltonian and, consequently, effective Hamiltonians and decay operators must be introduced to account for the configurations which have been neglected to construct the model-space nuclear wave function [19].

The quenching of the axial coupling constant g_A may have massive impact on the estimate of the half-life of $0\nu\beta\beta$ decay $T^{0\nu}_{1/2}$. Indeed, the latter is connected to the structure of the parent and granddaughter nuclei by way of the nuclear matrix element $M^{0\nu}$ according to the following expression:

$$\left[T^{0\nu}_{1/2}\right]^{-1} = G^{0\nu}|M^{0\nu}|^2 f(m_i, U_{ei})|^2, \tag{1}$$

$G^{0\nu}$ being the so-called phase-space factor (or kinematic factor) [20], and $f(m_i, U_{ei})$ accounting for the adopted model of $0\nu\beta\beta$ decay (light and/or heavy neutrino exchange, etc.) by way of the neutrino masses m_i and their mixing matrix elements U_{ei}. The explicit form of $f(m_i, U_{ei})$, within the mechanisms of light-neutrino exchange, is $f(m_i, U_{ei}) = g_A^2 \frac{\langle m_\nu \rangle}{m_e}$, where m_e is the electron mass, and $\langle m_\nu \rangle = \sum_i (U_{ei})^2 m_i$ is the effective neutrino mass.

The above expression evidences the strong dependence of the inverse half-life on the value of g_A, since it is determined by an exponent equal to 4, and the introduction of a quenching factor q may drastically reduce the probability of observing the $0\nu\beta\beta$ decay.

These considerations indicate that, in order to provide reliable calculations of the nuclear matrix elements involved in $0\nu\beta\beta$ decay, we need to achieve a robust knowledge of the renormalization mechanisms of decay operators that is grounded on a microscopic approach. To this end, since the $0\nu\beta\beta$ decay is ruled by the GT spin-isospin-dependent operator, a test for the predictiveness of nuclear structure calculations is the reproduction of observables such as β-decay amplitudes with neutrino emission, or a GT-strength distribution which can be obtained experimentally by way of intermediate-energy charge-exchange reactions.

The goal of deriving effective decay operators, that account for the degrees of freedom that have not been

explicitly included in the reduced model space, may be reached within the nuclear shell model (SM) by resorting to the many-body perturbation theory.

Arima, Towner, and their collaborators were forerunners in the study of the derivation of effective spin- and spin-isospin-dependent operators [18,21,22], exploiting both sources of the renormalization of shell-model $M1$ and GT transition operators, namely the role of meson-exchange currents as well as the derivation of effective operators accounting for the truncation of the Hilbert space to the SM space [19,23].

In this regard, it is worth mentioning the pioneering works of Kuo and his coworkers who, apart from the systematic development of the theory of the effective shell-model Hamiltonian ($H_{\rm eff}$) [24–26], considered for the first time the derivation of effective shell-model $0\nu\beta\beta$-decay operators and Hamiltonians starting from Paris [27] and Reid [28] nucleon-nucleon (NN) potentials [29,30].

Some of the authors of the present work started a few years ago a systematic study of the renormalization of the GT operator accounting for the reduced SM model space, but without considering the corrections arising from two-body electroweak currents [22,31]. Our theoretical framework has been the many-body perturbation theory [32–35], and effective shell-model GT operators and Hamiltonians for nuclei with mass ranging from $A = 48$ to $A = 136$ have been derived starting from the high-precision NN potential CD-Bonn [36], whose repulsive high-momentum components have been renormalized by way of the so-called $V_{\text{low-}k}$ approach [37]. The effective SM Hamiltonians and decay operators have reproduced quantitatively the spectroscopic and decay properties, such as the running sums of the GT strengths and nuclear matrix elements of the $2\nu\beta\beta$ decay ($M^{2\nu}$), without resorting to any quenching factor q, thus indicating the reliability of our theoretical approach [6,10,13].

Now, in the present paper, we report on a similar study of the derivation of the effective SM GT decay operator $\Theta_{\rm eff}$, but considering also the effect of the two-body electroweak currents to ascertain the relative weight of the latter with respect to the renormalization which accounts for the truncation of the full Hilbert space to the reduced model space. To this end, we start from chiral perturbation theory (ChPT), both for the nuclear Hamiltonian [38,39] as well as for the expansion of the electroweak currents which account for the composite structure of the nucleons [40–42]. This leads to a consistent way to construct the effective SM operators that are needed to construct the nuclear wave functions and calculate then the matrix elements of GT transitions. This approach has been extensively applied to light nuclear systems [43–47], and recently employed also to calculate the GT-decay strength for a few medium-mass nuclei in terms of *ab initio* methods [48].

The nuclear systems under our investigation, ^{48}Ca, ^{76}Ge, and ^{82}Se, are candidates for the observation of $0\nu\beta\beta$ decay. More precisely, we present here the results of the calculations of their GT-strength distributions and nuclear matrix elements of $2\nu\beta\beta$ decay, besides their low-energy spectroscopic properties, to validate the quality of our calculated nuclear wave functions. We have also performed the calculation of a large number of nuclear matrix elements of pure GT transitions between nuclei belonging to the $0f1p$-shell region, and compared them with the experimental ones extracted from the data of the observed $\log ft$ values.

As mentioned before, we start from a nuclear Hamiltonian based on ChPT [38,39], that consists of a high-precision two-nucleon (2N) potential derived at next-to-next-to-next-to-leading order (N^{3}LO) [49], and a three-nucleon (3N) component at N^{2}LO in ChPT [50]. The one- and two-body matrix elements of the axial currents have been derived through a chiral expansion up to N^{3}LO, and the low-energy constants (LECs) appearing in their expression are consistent with those of the nuclear potential we are starting from [49].

This is the first time a consistent treatment of the nuclear Hamiltonian and of the electroweak currents has been carried out, within the many-body perturbation theory, for nuclei that are $0\nu\beta\beta$-decay candidates.

This paper is organized as follows.

In Sec. II, first we sketch out briefly the nuclear Hamiltonian and electroweak currents we have started from, then we describe the perturbative approach to the derivation of the effective SM Hamiltonian and decay operators, that we have obtained considering ^{40}Ca and ^{56}Ni as doubly closed cores and the $0f1p$ and $0f_{5/2}1p0g_{9/2}$ orbitals as model spaces, respectively.

The results of the shell-model calculations are reported in Sec. III. First, we compare the calculated low-energy excitation spectra of parent and granddaughter nuclei involved in the double-β decays under consideration with the experimental counterparts. Since $H_{\rm eff}$ that we consider for the $0f1p$ shell was extensively investigated in a previous work [51], we validate also the new one for $0f_{5/2}1p0g_{9/2}$ model space by comparing the calculated and experimental yrast $J^\pi = 2^+$ excitation energies and two-neutron separation energies (S_{2n}) for nickel isotopes up to $N = 48$. Then, we report the results of the $2\nu\beta\beta$-decay matrix elements and GT transition-strength distributions for ^{48}Ca, ^{76}Ge, and ^{82}Se, as well as of nuclear matrix elements of GT transitions for about 40 nuclei belonging to the $0f1p$ shell.

Finally, in Sec. IV we summarize the conclusions of this study and also the outlook of our current research project.

II. THEORETICAL FRAMEWORK

A. The chiral nuclear Hamiltonian and electroweak currents

In the middle of the 1990s it was shown that chiral effective field theory (ChEFT) can provide a valuable tool to deal with hadronic interactions in a low-energy regime—like that of nuclear systems—with a systematic and model-independent approach [38,39]. As is well known, one has to start identifying a clear separation of scales [52], and for finite nuclei we can set the pion mass as the soft scale, $Q \sim m_\pi$, and the ρ mass as the hard scale, $\Lambda_\chi \sim m_\rho \sim 1$ GeV, which is also known as the chiral-symmetry breaking scale.

This is the starting point of a low-energy expansion arranged in terms of the soft scale over the hard scale, $(Q/\Lambda_\chi)^\nu$, where Q stands for an external momentum (nucleon three-momentum or pion four-momentum) or a pion mass, and the degrees of freedom are pions and nucleons and, eventually, their resonances (Δ).

The relevant feature of ChEFT is the link with its underlying theory, namely quantum chromodynamics; that is, the requirement to observe all relevant symmetries of QCD, specifically the broken chiral symmetry at low energies [53].

In this work, we consider the high-precision NN potential developed by Entem and Machleidt, by way of a chiral perturbative expansion at N^{3}LO [54], that is characterized by a regulator function whose cutoff parameter is $\Lambda = 500$ MeV.

An important advantage of the EFT approach to the derivation of a nuclear Hamiltonian is that it creates two- and many-body forces on an equal footing [39,55,56], since most interaction vertices that appear in the three-nucleon force (3NF) and in the four-nucleon force (4NF) also occur in the two-nucleon one (2NF).

It is worthwhile to point out that the first nonvanishing 3NF occurs at N^{2}LO. At this order, there are three 3NF topologies: the two-pion exchange (2PE), one-pion exchange (1PE), and three-nucleon-contact interactions. These terms are characterized by a set of low-energy constants (LECs): the 2PE contains the parameters c_1, c_3, and c_4 which, however, appear already in the 2PE component of the 2NF.

The 3NF 1PE contribution, apart from the parameters $g_A = 1.2723$, $f_\pi = 92.4$ MeV, $m_\pi = 138.04$ MeV, and $\Lambda_\chi = 700$ MeV, contains a new LEC c_D, while another new one, c_E, characterizes the 3N contact potential. These LECs, c_D and c_E, do not appear in the two-nucleon problem, and therefore they should be fixed to reproduce the observables of the $A = 3$ system. In present work, we have adopted the same c_D, c_E values as in Refs. [51,57–59], namely $c_D = -1$ and $c_E = -0.34$. This is a choice adopted in no-core shell model (NCSM) calculations in Ref. [50], where the authors first constrained the relation of c_D-c_E, and then investigated a set of observables in light p-shell nuclei to give a second constraint.

Another innovative feature of ChPT is the possibility of constructing electroweak currents, which account for the composite structure of the nucleons, by way of a perturbative expansion that is consistent with the derivation of the nuclear Hamiltonian we have just discussed [40–42,60–62].

This means that the one- and two-body matrix elements of the axial currents $\mathbf{J}_A$ are derived through a chiral expansion up to N^{3}LO, where the LECs appearing in their expression are consistent with those of the nuclear potential we have considered [49]. The details about the derivation of the axial currents within chiral effective theory can be found in Ref. [42].

Here, we report the expression of $\mathbf{J}_A$ up to N^{3}LO in the limit of vanishing momentum transfer, while its diagrammatic expansion is illustrated in Fig. 1.

The expansion of the electroweak current $\mathbf{J}_A$ up to N^{3}LO contains one- and two-body contributions, and therefore can be written as

$$\mathbf{J}_A = \mathbf{J}_A(1b) + \mathbf{J}_A(2b). \tag{2}$$

The one-body contributions to $\mathbf{J}_A$ appear at the LO and N^{2}LO of the ChPT expansion. The LO term, shown in Fig. 1(a), is the standard GT operator (with a minus sign) given by

$$\mathbf{J}^{\rm LO}_{A,\pm} = -g_A \sum_i \boldsymbol{\sigma}_i \tau_{i,\pm}, \tag{3}$$

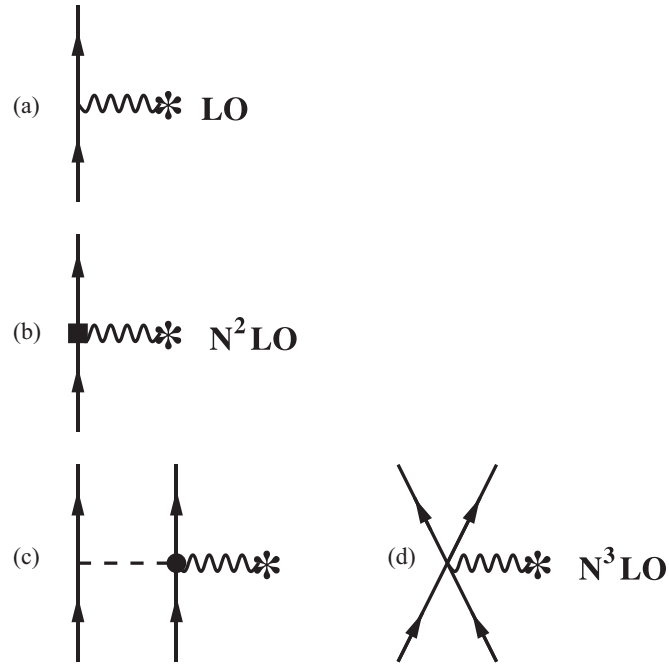

FIG. 1. Diagrams illustrating the contributions up to N^{3}LO to the axial current we have considered in the present work. The wavy lines represent the external weak field, the dashed lines the pion exchange, the square in diagram (b) represents relativistic corrections, while the dot in diagram (c) denotes a vertex induced by subleading terms in the π-nucleon chiral Lagrangian.

where $g_A = 1.2723$, and σ_i and τ_i are the Pauli spin and isospin operators of the ith nucleon, having specified the charge-rising $(+)$ and charge-lowering $(-)$ cases defined by

$$\tau_{i,\pm} = (\tau_{i,x} \pm i\tau_{i,y})/2. \tag{4}$$

The N^{2}LO term [see Fig. 1(b)] consists of a relativistic correction to the GT operator:

$$\mathbf{J}^{\rm N^2LO}_{A,\pm} = \frac{g_A}{2m_N^2} \sum_i \mathbf{K}_i \times (\boldsymbol{\sigma}_i \times \mathbf{K}_i)\tau_{i,\pm}, \tag{5}$$

where m_N is the nucleon mass and

$$\mathbf{K}_i = (\mathbf{p}'_i + \mathbf{p}_i)/2, \tag{6}$$

$\mathbf{p}_i$ ($\mathbf{p}'_i$) being the initial (final) momentum of the nucleon i.

The first two-body diagrams appear at N^{3}LO of the ChPT expansion, where we have the 1PE contribution [Fig. 1(c)] and the contact term (CT) [Fig. 1(d)], as given by

$$\begin{aligned}\mathbf{J}^{\rm N^3LO}_{A,\pm}(1{\rm PE};\mathbf{k}) = \sum_{i<j} \frac{g_A}{2f_\pi^2} \Bigg\{ & 4c_3 \tau_{j,\pm}\mathbf{k} + (\boldsymbol{\tau}_i \times \boldsymbol{\tau}_j)_\pm \\ & \times \left[\left(c_4 + \frac{1}{4m} \right) \boldsymbol{\sigma}_i \times \mathbf{k} - \frac{i}{2m} \mathbf{K}_i \right] \Bigg\} \boldsymbol{\sigma}_j \cdot \\ & \times \mathbf{k} \frac{1}{\omega_k^2} + (i \rightleftharpoons j),\end{aligned} \tag{7}$$

$$\mathbf{J}^{\rm N^3LO}_{A,\pm}({\rm CT};\mathbf{k}) = \sum_{i<j} z_0 (\boldsymbol{\tau}_i \times \boldsymbol{\tau}_j)_\pm (\boldsymbol{\sigma}_i \times \boldsymbol{\sigma}_j), \tag{8}$$

where ω_k is defined by the relation $\omega_k^2 = k^2 + m_\pi^2$ and, since the external field momentum is vanishing, we have that

$$\mathbf{k}_i = (\mathbf{p}'_i - \mathbf{p}_i)/2 = -\mathbf{k}_j = \mathbf{k}. \tag{9}$$

Moreover, we have defined

$$(\boldsymbol{\tau}_i \times \boldsymbol{\tau}_j)_\pm = (\boldsymbol{\tau}_i \times \boldsymbol{\tau}_j)_x \pm i(\boldsymbol{\tau}_i \times \boldsymbol{\tau}_j)_y, \tag{10}$$

and

$$z_0 = \frac{g_A}{2f_\pi^2 m_N}\left[-\frac{m_N}{4g_a\Lambda_\chi}c_D + \frac{m_N}{3}(c_3 + 2c_4) + \frac{1}{6}\right]. \tag{11}$$

The above equation shows that the 1PE term [Eq. (7)] contains the c_3 and c_4 LECs, which determine the two-pion exchange contribution of the chiral 3NF at N^{2}LO, while in the CT term [Eq. (8)] there appear, along with c_3 and c_4, also c_D [Eq. (11)] that is connected to the 3NF one-pion exchange contribution appearing at N^{2}LO for the nuclear Hamiltonian.

Finally, the configuration-space expression for the two-body contribution of $\mathbf{J}_A$ is obtained as

$$\mathbf{J}_{A,\pm}(2b) = \int \frac{d\mathbf{k}}{(2\pi)^3} e^{i\mathbf{k}\cdot\mathbf{r}_{ij}} C_\Lambda(k) \mathbf{J}_{A,\pm}(2b;\mathbf{k}), \tag{12}$$

where $\mathbf{r_{ij}} = \mathbf{r_i} - \mathbf{r_j}$, $C_\Lambda(k) = e^{-(k/\Lambda)^4}$ is the regulator function, and K_j is replaced by $-i\nabla_j$ in $\mathbf{J}_{A,\pm}(2b;\mathbf{k})$.

We have calculated the matrix elements of these two-body terms in the harmonic-oscillator (HO) basis, consistently with the chiral Hamiltonian, and added them to the one-body LO and N^{2}LO operators.

It is worth pointing out that, as will be shown in Sec. II C, we have included these two-body electroweak currents explicitly and without resorting to any approximation. This is at variance with respect to the procedure that was followed in Ref. [63], where the chiral two-body axial currents were included, retaining only the normal-ordered one-body contribution by taking as reference state a Fermi-gas approximation for the core.

The convergence with respect to the truncation of the ChPT expansion at N^{3}LO will be discussed in Sec. III.

B. The effective shell-model Hamiltonian

The nuclear Hamiltonian, that includes 2NF and 3NF components, is the foundation to build up the effective SM Hamiltonian $H_{\rm eff}$, namely the single-particle (SP) energies and two-body matrix elements (TBMEs) of the residual interaction, which are the basic inputs to solve the SM eigenvalue problem. $H_{\rm eff}$ must account for the degrees of freedom that are not explicitly included in the truncated Hilbert space of the configurations (the model space), that in our case is spanned by the proton/neutron $0f1p$ orbitals outside the doubly closed ^{40}Ca, or by the proton/neutron $0f_{5/2}1p0g_{9/2}$ orbitals outside the ^{56}Ni core.

This goal may be pursued by a similarity transformation which arranges, within the full Hilbert space of the configurations, a decoupling of the model space P where the valence nucleons are constrained from its complement $Q = 1 - P$.

This problem may be tackled within the time-dependent perturbation theory, namely by expressing $H_{\rm eff}$ through the Kuo-Lee-Ratcliff folded-diagram expansion in terms of the $\hat{Q}$-box vertex function [26,35,64].

The $\hat{Q}$ box is defined in terms of the full nuclear Hamiltonian $H = H_0 + H_1$, where H_0 represents the unperturbed component, obtained by the introduction of the harmonic-oscillator auxiliary potential, and H_1 corresponds to the residual interaction, as

$$\hat{Q}(\epsilon) = PH_1P + PH_1Q\frac{1}{\epsilon - QHQ}QH_1P, \tag{13}$$

where ϵ is an energy parameter called "starting energy."

An exact calculation of the $\hat{Q}$ box is practically impossible, but the term $1/(\epsilon - QHQ)$ is amenable to be expanded as a power series,

$$\frac{1}{\epsilon - QHQ} = \sum_{n=0}^{\infty} \frac{1}{\epsilon - QH_0Q}\left(\frac{QH_1Q}{\epsilon - QH_0Q}\right)^n, \tag{14}$$

leading to the perturbative expansion of the $\hat{Q}$ box. It is worth introducing a diagrammatic representation of the $\hat{Q}$-box perturbative expansion, as a collection of irreducible valence-linked Goldstone diagrams [25].

The $\hat{Q}$ box is then employed to solve nonlinear matrix equations to derive $H_{\rm eff}$ by way of iterative techniques such as the Kuo-Krenciglowa and Lee-Suzuki ones [65], or graphical noniterative methods [66]. We have verified that the latter provide a faster and more stable convergence to the solution of $H_{\rm eff}$, and these are the techniques we have employed in present work.

In order to derive our $H_{\rm eff}$'s, we include in our $\hat{Q}$-box expansion one- and two-body Goldstone diagrams through third order in the two-nucleon potential and up to first order in the three-nucleon (NNN) one. In Ref. [34] a complete list of diagrams with NN vertices can be found. The diagrams at first order in the NNN potential, as well as their analytical expressions, are reported in Refs. [51,57]. It should be noted that these expressions are the coefficients of the one-body and two-body terms arising from the normal-ordering decomposition of the three-body component of a many-body Hamiltonian [67]. In Ref. [68], Holt and coworkers showed that the uncertainty linked to neglecting higher-order contributions from NNN vertices (residual NNN forces) is small.

An important issue that has to be stressed is the fact that the nuclear systems we are going to investigate are characterized by many valence nucleons, and this means that one should derive many-body $H_{\rm eff}$'s which depend on the number of valence particles. This implies that the $\hat{Q}$ box should include at least contributions from three-body diagrams accounting for the three-body interaction induced by the 2NF between the valence nucleons and the configurations outside the model space.

The tool we employ to diagonalize the SM Hamiltonian is the KSHELL code [69], which cannot perform the diagonalization of a three-body $H_{\rm eff}$. Then, we derive a density-dependent two-body term from the three-body contribution arising from the calculation of nine one-loop diagrams (see the graphs in Fig. 8 of Ref. [35]) at second order in perturbation theory [70].

We reported their explicit form in Ref. [51], and it depends on the unperturbed occupation density ρ of the external valence line that has been summed on. This leads to the derivation of density-dependent $H_{\rm eff}$'s which account for the number of valence protons and neutrons, and differ only in their TBMEs, since these one-loop diagrams are two-body terms.

An extensive report about the perturbative behavior of the $\hat{Q}$-box expansion, starting from the chiral N^{3}LO potential of Entem and Machleidt, was reported in Ref. [51], which discussed both its order-by-order convergence properties and the convergence with respect to the dimension of the space of the intermediate states, considering the systems with one and two valence neutrons, namely ^{41}Ca and ^{42}Ca, respectively. It is worth recalling here that the number of intermediate states is expressed as a function of the maximum allowed excitation energy of the intermediate states in terms of the oscillator quanta $N_{\rm max}$ [34], and includes intermediate states with an unperturbed excitation energy up to $E_{\rm max} = N_{\rm max}\hbar\omega$. The present limitation of our computing resources allows us to include, for both ^{40}Ca and ^{56}Ni cores, a maximum number of intermediate states that does not exceed $N_{\rm max} = 18$.

Actually, in Ref. [51] we pointed out that while the energy spacings of the theoretical SP spectra converge quite rapidly as a function of the number of intermediate states, this convergence cannot be reached with the larger value of the oscillator quanta we may consider $N_{\rm max} = 18$, when calculating their absolute values with respect to the closed cores ^{40}Ca, ^{56}Ni.

Then, for the calculations of ground-state energies of nuclei in the $0f1p$ region, we have fixed the SP energies of proton and neutron $0f_{7/2}$ orbitals at -1.1 and -8.4 MeV, respectively. For the $H_{\rm eff}$'s that have been constructed with respect to the ^{56}Ni core, the SP energies of proton and neutron $1p_{3/2}$ have been chosen to be -0.7 and -10.2 MeV, respectively. Those values are consistent with experimental values of ^{41}Sc and ^{41}Ca, with respect to ^{40}Ca, and of ^{57}Cu and ^{57}Ni, with respect to ^{56}Ni [71].

The Coulomb potential is explicitly taken into account, and summed to the matrix elements of the NN potential. The oscillator parameter $\hbar\omega$ we have employed to compute the matrix elements of the NN and NNN potentials in the HO basis is equal to 11 and 10 MeV for ^{40}Ca and ^{56}Ni cores, respectively, according to the expression $\hbar\omega = 45A^{-1/3} - 25A^{-2/3}$ [72].

C. Effective shell-model transition operators

One of the goals of this work is the calculation of the matrix elements of quadrupole-electric transition and GT-decay operators Θ which are connected to measurable quantities such as $B(E2)$, GT strengths, and the nuclear matrix element of the $2\nu\beta\beta$ decay, $M^{2\nu}$.

The diagonalization of $H_{\rm eff}$ provides the projections of the true nuclear wave functions onto the chosen model space P; then we need to renormalize any transition/decay operator Θ to account for the neglected degrees of freedom corresponding to the Q space.

The procedure that we apply to calculate effective SM operators is the one introduced by Suzuki and Okamoto in Ref. [33]. This approach to the derivation of effective transition/decay operators $\Theta_{\rm eff}$ is consistent with the one we have described in the previous section to construct $H_{\rm eff}$, namely it is based on perturbative expansion of a vertex function $\hat{\Theta}$ box, analogously with the derivation of $H_{\rm eff}$ in terms of the $\hat{Q}$ box. The details of such a procedure may be found in Ref. [35], and in the following we only sketch out the main building blocks.

First, we expand perturbatively the two energy-dependent vertex functions,

$$\hat{\Theta}(\epsilon) = P\Theta P + P\Theta Q\frac{1}{\epsilon - QHQ}QH_1P,$$

$$\hat{\Theta}(\epsilon_1;\epsilon_2) = PH_1Q\frac{1}{\epsilon_1 - QHQ}Q\Theta Q\frac{1}{\epsilon_2 - QHQ}QH_1P,$$

and their energy derivatives for $\epsilon = \epsilon_0$, ϵ_0 being the unperturbed energy of the degenerate model space:

$$\hat{\Theta}_m = \frac{1}{m!}\frac{d^m\hat{\Theta}(\epsilon)}{d\epsilon^m}\bigg|_{\epsilon=\epsilon_0},$$

$$\hat{\Theta}_{mn} = \frac{1}{m!n!}\frac{d^m}{d\epsilon_1^m}\frac{d^n}{d\epsilon_2^n}\hat{\Theta}(\epsilon_1;\epsilon_2)\bigg|_{\epsilon_1=\epsilon_0,\epsilon_2=\epsilon_0}.$$

Then, we can calculate a series of operators χ_n:

$$\chi_0 = (\hat{\Theta}_0 + \text{H.c.}) + \hat{\Theta}_{00}, \tag{15}$$

$$\chi_1 = (\hat{\Theta}_1\hat{Q} + \text{H.c.}) + (\hat{\Theta}_{01}\hat{Q} + \text{H.c.}),$$

$$\chi_2 = (\hat{\Theta}_1\hat{Q}_1\hat{Q} + \text{H.c.}) + (\hat{\Theta}_2\hat{Q}\hat{Q} + \text{H.c.}) + (\hat{\Theta}_{02}\hat{Q}\hat{Q} + \text{H.c.}) + \hat{Q}\hat{\Theta}_{11}\hat{Q},$$

$$\vdots \tag{16}$$

The effective operator $\Theta_{\rm eff}$ is then expressed in terms of an expansion of the χ_n operators as follows:

$$\Theta_{\rm eff} = H_{\rm eff}\hat{Q}^{-1}(\chi_0 + \chi_1 + \chi_2 + \cdots). \tag{17}$$

We arrest the χ_n series at $n = 2$, and the $\hat{\Theta}$ vertex functions are expanded up to third order in perturbation theory, and in Refs. [10,73,74] we have tackled the issue of the convergence of the χ_n series and of the perturbative expansion of the $\hat{\Theta}$ box, showing that this truncation is substantially satisfying. Figure 10 of Ref. [35] and Fig. 1 of Ref. [74] show all the diagrams up to second order appearing in the $\hat{\Theta}(\epsilon_0)$ expansion for a one-body operator $\Theta^{\rm 1b}$ and two-body one $\Theta^{\rm 2b}$.

In the present work, the decay operators Θ are the one-body electric-quadrupole ($E2$) transitions $q_{p,n}r^2Y^2_m(\hat{r})$ (the charge $q_{p,n}$ being e for protons and 0 for neutrons) and the axial electroweak currents $\mathbf{J}_A$ that we employ to calculate the nuclear matrix elements for GT decays.

We have shown in the previous section that, regarding the effective operator for GT decays, electroweak currents have one- and two-body components, and consequently the effective SM operator has the same structure. Moreover, the first-order term of the one-body component includes also a normal-ordered contribution, calculated with respect to the closed-core reference state, obtained from the two-body matrix elements of the electroweak currents.

Our perturbative expansion of the $\hat{\Theta}$ box includes contributions up to third order in the many-body perturbation theory

for the one-body components (for both $E2$ transitions and GT decays), and up to second order for the two-body component of the effective GT decay operator.

It is worth also reporting the explicit expression of the nuclear matrix elements of the single-GT and $2\nu\beta\beta$ decays in terms of the axial electroweak currents:

$$M^{1\nu}_{\rm GT} = \langle J_f||\mathbf{J}^{\mathcal{I}}_A||J_i\rangle, \tag{18}$$

$$M^{2\nu}_{\rm GT} = \sum_n \frac{\langle 0^+_f||\mathbf{J}^{\mathcal{I}}_A||1^+_n\rangle\langle 1^+_n||\mathbf{J}^{\mathcal{I}}_A||0^+_i\rangle}{E_n + E_0}. \tag{19}$$

where the superscript $\mathcal{I}$ indicates that we are employing the matrix elements of either the bare or the effective GT decay operators.

In the above equations, E_n is the excitation energy of the $J^\pi = 1^+_n$ intermediate state, and $E_0 = \frac{1}{2}Q_{\beta\beta}(0^+) + \Delta M$, where $Q_{\beta\beta}(0^+)$ and ΔM are the Q value of the transition and the mass difference of the parent and daughter nuclear states, respectively. The index n runs over all possible intermediate states induced by the given transition operator. It should be pointed out that we have not considered in our calculations the Fermi component of the β-decay operator since it plays a marginal role [75,76] and in most calculations is neglected altogether.

The calculation of $M^{2\nu}$ has been carried out by way of the Lanczos strength-function method [77], since this is the most efficient way to include a number of $J^\pi = 1^+$ intermediate states that is sufficient to provide the needed accuracy.

Then, the calculated value of $M^{2\nu}$ can be compared with the experimental counterpart, which is extracted from the observed half life $T^{2\nu}_{1/2}$:

$$\left[T^{2\nu}_{1/2}\right]^{-1} = G^{2\nu}\left|M^{2\nu}_{\rm GT}\right|^2, \tag{20}$$

$G^{2\nu}$ being the $2\nu\beta\beta$-decay phase-space (or kinematic) factor [20,78].

III. RESULTS

In this section we present the results of our SM calculations. First, to validate the quality of the nuclear wave functions we employ to describe GT decays, we compare the theoretical low-energy spectroscopic properties of a few nuclei, in the mass regions which are of relevancy for the $H_{\rm eff}$'s we have derived, with the experimental ones. In Refs. [51,58,59] we have already shown the ability of the $0f1p$-shell $H_{\rm eff}$'s that we have derived, starting from the chiral nuclear Hamiltonian we presented in Sec. II A, to reproduce accurately the low-energy spectra and monopole properties of calcium, titanium, chromium, iron, and nickel isotopes.

Therefore, in Sec. III A 1 we limit our discussion only to the $H_{\rm eff}$'s we have constructed for the $0f_{5/2}1p0g_{9/2}$ model space, focusing on their monopole properties. It is worth emphasizing that, since we derive $H_{\rm eff}$ considering the contribution of the induced three-nucleon potential too, as reported in Sec. II B, we use a different $H_{\rm eff}$ for each nuclear system.

In the Supplemental Material [79] the effective SM Hamiltonian for $A = 58$ systems, namely for one- and two-valence nucleon systems, can be found.

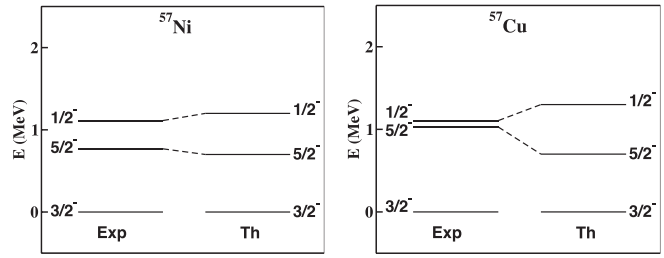

FIG. 2. Comparison between experimental and calculated SP spectra of ^{57}Ni and ^{57}Cu.

In Sec. III A 2 we present the results of the calculation of the low-energy spectroscopic properties of the parent and granddaughter nuclei that are involved in the double-β decay processes we consider in this paper, namely ^{48}Ca, ^{48}Ti, ^{76}Ge, ^{76}Se, ^{82}Se, and ^{82}Kr, and compare them with available data.

Finally, in Sec. III B we compare with experiment the calculated properties related to the GT decay, such as the nuclear matrix elements of about 40 nuclear systems in the $0f1p$-shell region, the GT$^-$ strength distributions, and the $M^{2\nu}$'s of the above mentioned nuclei.

A. Calculation of the spectroscopic properties

1. Monopole properties of $H_{\rm eff}$ in the $0f_{5/2}1p0g_{9/2}$ model space

As previously mentioned, the effective SM Hamiltonian for $A = 58$ nuclei can be found in the Supplemental Material of this paper, and the values of our calculated SP energies are $\epsilon_{1p3/2} = 0.0$ MeV, $\epsilon_{0f5/2} = 0.7$ MeV, $\epsilon_{1p1/2} = 1.3$ MeV, and $\epsilon_{0g/2} = 6.2$ MeV for the proton orbitals, and $\epsilon_{1p3/2} = 0.0$ MeV, $\epsilon_{0f5/2} = 0.7$ MeV, $\epsilon_{1p1/2} = 1.2$ MeV, and $\epsilon_{0g/2} = 6.1$ MeV for the neutron orbitals.

Since the SP energies are the eigenvalues of the $H_{\rm eff}$'s for the single-valence-nucleon systems, from the SM perspective these numbers correspond to the excitation energies of the SP states in ^{57}Cu and ^{57}Ni. In Fig. 2 we compare the theoretical and experimental SP spectra of these two nuclei [80]; note that there is no firm assignation of a $J^\pi = 9/2^+$ SP state for either of them.

From the inspection of Fig. 2, we observe that the calculated SP energies reproduce quite well the observed natural-parity SP spacings. As a test case of the isotopic chains belonging to the $0f_{5/2}1p0g_{9/2}$ model space, we examine the nickel isotopes, whose study is pivotal to investigate the shell-closure properties of our calculated $H_{\rm eff}$'s.

In Fig. 3 we show the behavior of the calculated and experimental $J^\pi = 2^+_1$ excitation energies of nickel isotopes up to $N = 48$ [80]. The black dashed line indicates the results obtained with the $A = 58$ effective Hamiltonian (see the Supplemental Material [79]), and the black solid line refers to the results obtained with density-dependent $H_{\rm eff}$'s accounting for the induced three-body potential (see Sec. II B).

As can be seen, the theoretical results follow quite well the observed behavior of the yrast $J^\pi = 2^+$ states all along the isotopic chain, except for the energy bump at $N = 32$ which is a fingerprint of the subshell closure of the neutron $1p_{3/2}$ orbital, thus revealing that the $Z = 28$ cross-shell excitations

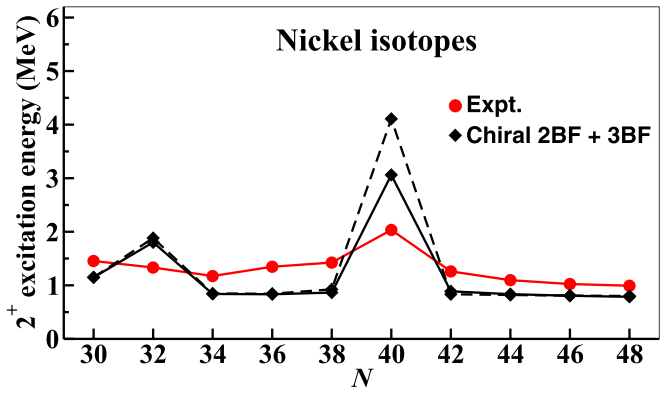

FIG. 3. Experimental and calculated excitation energies of the yrast $J^\pi = 2^+$ states for nickel isotopes from $N = 30$ to 48. The black dashed line refers to results obtained with the $H_{\rm eff}$ for the $A = 58$ system (see text for details).

still play an important role in describing the low-energy spectroscopy of light nickel isotopes [81].

It should be noted that our SM calculations reproduce the shell closure at $N = 40$ (^{68}Ni), the result being remarkably better by employing the density-dependent $H_{\rm eff}$'s. This confirms the ability of the monopole component of our $H_{\rm eff}$'s to provide the observed shell evolution, a feature that may be ascribed to the NNN component of the chiral nuclear Hamiltonian, as we showed in our previous study of $0f1p$-shell nuclei [51].

Similar positive conclusions may be drawn from the inspection of the behavior of the nickel two-neutron separation energies (S_{2n}) as a function of the neutron number, which we have reported in Fig. 4. We note that the discrepancy between the results obtained with $A = 58 H_{\rm eff}$ (dashed black line) and the density-dependent $H_{\rm eff}$'s (solid black line) starts to enlarge at $N = 44$, but from that point on there are only extrapolated values and no experimental counterpart.

We have pointed out in our previous study of nuclear systems belonging to the $0f1p$-shell region that a major role in

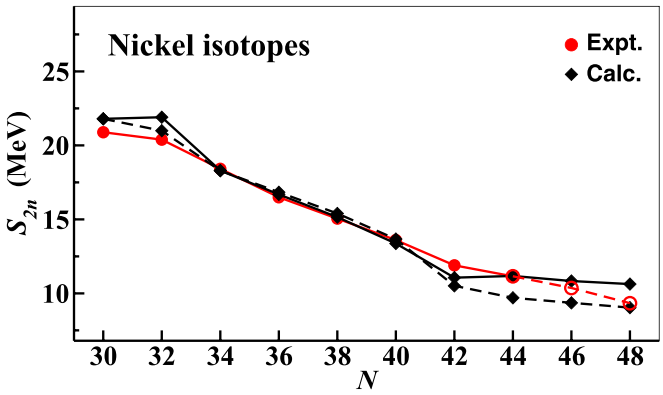

FIG. 4. Experimental and calculated two-neutron separation energies for nickel isotopes from $N = 30$ to 48. The black dashed line refers to results obtained with the $H_{\rm eff}$ for the $A = 58$ system (see text for details). Data are taken from [71]; open circles correspond to estimated values.

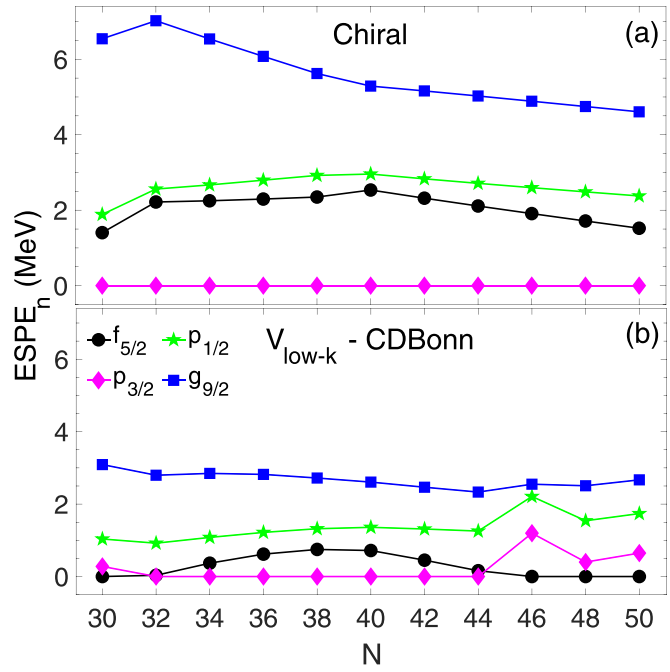

FIG. 5. Neutron ESPEs from $H_{\rm eff}$ TBMEs for nickel isotopes as a function of the neutron number, calculated from the CD-Bonn potential and from chiral two- and three-body potential (see the text for details).

driving the shell evolution, starting from chiral ChPT nuclear Hamiltonians, is played by 3BF that contribute significantly to the monopole component of $H_{\rm eff}$ [51]. The direct link between the properties of the monopole component and the shell evolution is provided by the calculation and the study of the effective single-particle energy (ESPE) that is defined in terms of the bare SP energy ϵ_j and the monopole part of the TBMEs [82,83]:

$$\mathrm{ESPE}(j) = \epsilon_j + \sum_{j'} V^{\rm mon}_{jj'} n_{j'}, \tag{21}$$

where the sum runs over the model-space levels j', n_j being the occupation number of particles in the level j obtained from the diagonalization of the shell-model Hamiltonian, and the angular-momentum-averaged monopole component of the SM Hamiltonian is defined through the TBMEs of the SM residual interaction $V_{\rm eff}$ as follows:

$$V^{\rm mon}_{ij} = \frac{\sum_J (2J+1)\langle i, j|V_{\rm eff}|i, j\rangle_J}{\sum_J (2J+1)}\,.$$

To illustrate the connection between the evolution of the ESPEs as a function of the valence nucleons and the closure properties of $H_{\rm eff}$'s, in Fig. 5 we compare the neutron ESPEs of nickel isotopes obtained with two different $H_{\rm eff}$'s, both of them defined in the $0f_{5/2}$, $1p$, $0g_{9/2}$ model space: the $H_{\rm eff}$ we have derived for the present work from chiral 2NF and 3NF, and that which was constructed and employed in Ref. [10] starting from the CD-Bonn high-precision NN potential [36] renormalized by way of the $V_{\text{low-}k}$ procedure [37]. Black dots, magenta diamonds, green stars, and blue squares indicate the $0f_{5/2}$, $1p_{3/2}$, $1p_{1/2}$, and $0g_{9/2}$ ESPEs, respectively.

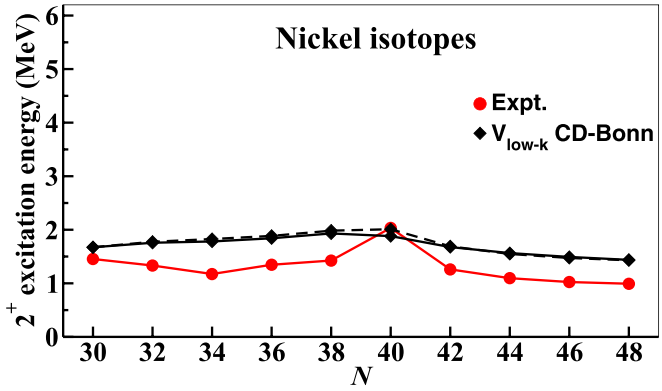

FIG. 6. Same as in Fig. 3, but the theoretical results are here obtained with $H_{\rm eff}$ reported in Ref. [10] (see text for details).

The inspection of Fig. 5 shows that the $H_{\rm eff}$ from the ChPT Hamiltonian generates ESPEs that are characterized by an almost constant energy splitting along the istopic chain, the $0g_{9/2}$ ESPE being always well separated from the other ones. This behavior of the ESPEs is reflected in the neutron closure at $N = 40$, as emerges from the results in Fig. 3.

The situation is different when considering the ESPEs obtained from the $H_{\rm eff}$ that was employed in Ref. [10], where the energy splittings are strongly reduced, exposing then the shell evolution to the correlations induced by higher-multipole components of the residual two-body potential. This feature is reflected by a collective flat behavior of the calculated excitation energies of the yrast $J^\pi = 2^+$ states, as can be seen in Fig. 6, reaching the climax with the disappearance $N = 40$ closure.

2. *Low-energy spectra of* ^{48}Ca, ^{48}Ti, ^{76}Ge, ^{76}Se, ^{82}Se, *and* ^{82}Kr

Before starting the analysis of the calculated quantites related to the GT decay, we deem it is worth comparing our calculated low-energy spectra of ^{48}Ca, ^{48}Ti, ^{76}Ge, ^{76}Se, ^{82}Se, and ^{82}Kr, as well as their electromagnetic-transition properties, with the available experimental counterparts.

All calculations have been performed employing theoretical SP energies, TBMEs, and effective transition operators, following the procedure described in Secs. II B and II C. The TBMEs include the contribution of induced three-body forces, so they depend on the different nuclear system under consideration (see the content in Sec. II B).

The shell-model calculation for ^{48}Ca and ^{48}Ti are performed within the full fp shell, namely the proton and neutron $0f_{7/2}$, $0f_{5/2}$, $1p_{3/2}$, and $1p_{1/2}$ orbitals. In Fig. 7, we show the experimental [80] and calculated low-energy spectra of ^{48}Ca and ^{48}Ti. Next to the arrows, whose widths are proportional to the $B(E2)$ strengths, we report the numerical values in e^2fm^4 [80].

As can be seen, we reproduce very nicely the observed shell closure of the neutron $0f_{7/2}$ orbital in ^{48}Ca, the agreement between the experimental and calculated spectra may be considered quantitative, and also the observed $B(E2)$s are satisfactorily reproduced by the theory.

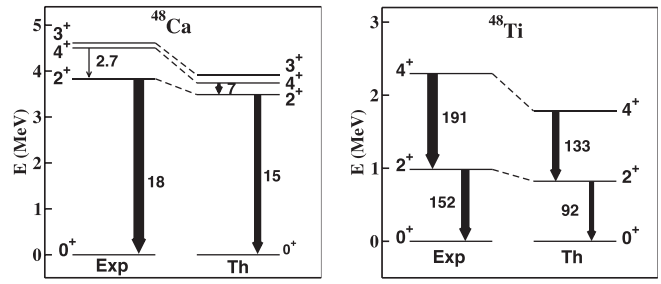

FIG. 7. Experimental and calculated spectra of ^{48}Ca and ^{48}Ti. $B(E2)$ strengths (in e^2fm^4) are also reported (see text for details).

As already pointed out in the previous sections, the shell-model calculations for ^{76}Ge, ^{76}Se, ^{82}Se, and ^{82}Kr have been performed within the model space spanned by the four proton and neutron orbitals $0f_{5/2}$, $1p_{3/2}$, $1p_{1/2}$ and $0g_{9/2}$, considering ^{56}Ni as a closed core. The experimental [80] and calculated low-energy spectra of ^{76}Ge and ^{76}Se are reported in Fig. 8, together with the experimental [80] and calculated $B(E2)$ strengths (in e^2fm^4).

We notice that while the agreement between the experimental and calculated spectra and $B(E2)$'s for ^{76}Se is quite satisfactory, the same conclusion does not apply to ^{76}Ge, whose observed collectivity is poorly described. These results are at variance with respect to those we found in Ref. [10], where the $H_{\rm eff}$ was derived from a $NNV_{\text{low-}k}$ potential obtained from the CD-Bonn potential [36], and the reproduction of the ^{76}Ge spectrum and $B(E2)$'s was far better than the one in Fig. 8.

There is experimental evidence that low-energy states of ^{76}Ge reveal a rigid triaxial deformation [84], and this enhanced collectivity, that characterizes heavy-mass germanium isotopes, may be reproduced within shell model by employing a model space larger than the $0f_{5/2}1p0g_{9/2}$ one [85].

The different collective behavior of the calculated ^{76}Ge low-lying energy spectrum, as obtained with present the chiral $H_{\rm eff}$ and the one in Ref. [10], traces back to their different monopole components. In Table I we report the proton and neutron ESPEs for ^{76}Ge, calculated with both $H_{\rm eff}$'s, and it is evident that the SM Hamiltonian employed in Ref. [10] provides an ESPE spectrum more compressed than the one obtained with the chiral $H_{\rm eff}$.

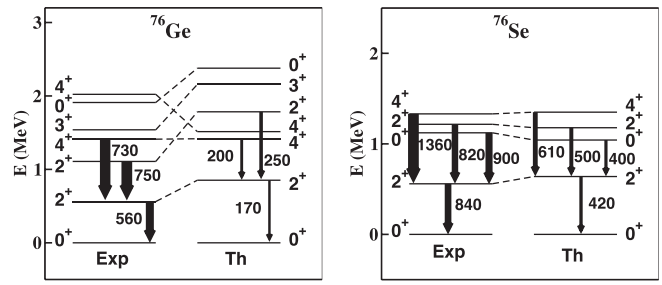

FIG. 8. Same as in Fig. 7, but for ^{76}Ge and ^{76}Se (see text for details).

TABLE I. Proton and neutron ESPEs (in MeV) for ^{76}Ge calculated with the $H_{\rm eff}$'s derived from the chiral 2NF and 3NF (this work), and from the $V_{\text{low-}k}$ potential obtained from the CD-Bonn potential [10].

	Proton		Neutron	
Orbital	Chiral	$V_{\text{low-}k}$	Chiral	$V_{\text{low-}k}$
$0f_{5/2}$	2.9	0.3	3.6	0.5
$1p_{3/2}$	0.0	0.0	0.0	0.0
$1p_{1/2}$	3.1	0.9	3.1	1.3
$09_{9/2}$	7.0	3.3	6.3	2.5

The collectivity induced by the smaller energy spacings of the ESPEs, that are calculated starting from the $V_{\text{low-}k}$ renormalization of the CD-Bonn potential, has a drawback: in a few cases this feature fails to reproduce shell closures, such as in ^{48}Ca (see Fig. 5 in Ref. [10]) or in ^{68}Ni, as we have shown in Fig. 6.

Also, for the shell model calculation of ^{82}Se and ^{82}Kr, we have considered the $0f_{5/2}1p0g_{9/2}$ model space, and in Fig. 9 we report the experimental [80] and theoretical low-energy spectra and $B(E2)$'s.

There is little to comment; the agreement between theory and experiment, especially as regards the electromagnetic properties, can be considered very satisfactory, with the exception of the inversion in the calculated spectra of the 0_2^+ states with respect to the 2_2^+ and 4_1^+ ones.

B. Nuclear matrix elements of the GT decay

In this section, we present the results of our calculations of GT nuclear matrix elements and GT$^-$ strength distributions for ^{48}Ca, ^{76}Ge, and ^{82}Se, and compare them with the available data.

In order to assess the distinct role that is played by the meson-exchange currents—that are taken into account by ChPT expansion of the axial current—and by the configurations outside the model space in the renormalization of the shell-model GT-decay operator, we label our calculations as follows:

(a) calculations performed by employing the bare $\mathbf{J}_A$ at LO in ChPT, namely the usual spin-isospin dependent GT operator $g_A\boldsymbol{\sigma}\cdot\boldsymbol{\tau}$;

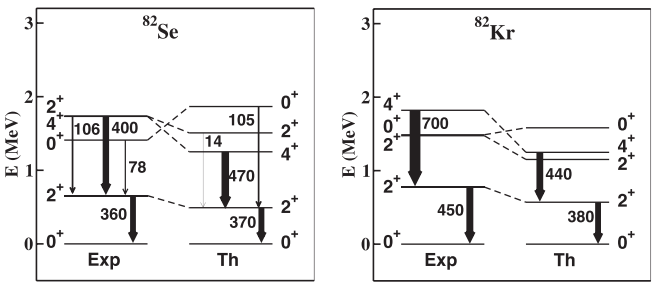

FIG. 9. Same as in Fig. 7, but for ^{82}Se and ^{82}Kr.

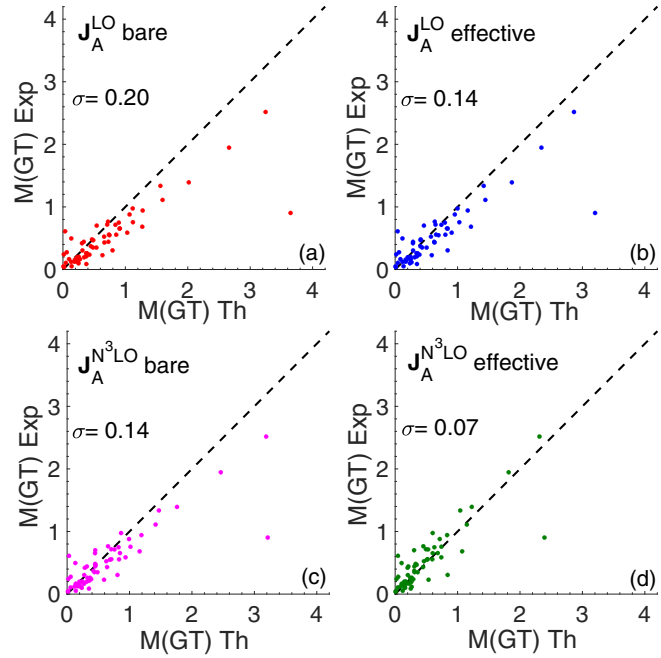

FIG. 10. Correlation plots between experimental (y axis) and calculated (x axis) values of the GT nuclear matrix elements of a few decay processes in the $0f1p$ shell region. The experimental values are taken from Ref. [80].

(b) calculations performed by employing the effective $\mathbf{J}_A$ at LO in ChPT, that accounts for the contributions of configurations outside the model space (see Sec. II C);

(c) calculations performed by employing the bare $\mathbf{J}_A$ at N^{3}LO in ChPT, that includes also the contributions of the relativistic corrections to the GT operator and the two-body contact and pion-exchange contributions;

(d) calculations performed by employing the effective $\mathbf{J}_A$ at N^{3}LO in ChPT, a SM operator that has both one- and two-body components.

First, we have considered 60 experimental GT decays of 43 nuclei belonging to the region of the $0f1p$ shell [80], involving only yrast states, and compared the matrix elements extracted from the data with our calculated values. We report them in a correlation plot in Fig. 10, where the theoretical nuclear matrix elements are obtained employing SM GT decay operators (a)–(d), together with the root-mean-square deviation σ:

$$\sigma = \sqrt{\frac{\sum_{i=1}^{n}(x_i - \hat{x}_i)^2}{n}},$$

x_i being the experimental GT nuclear matrix element, $\hat{x}_i$ the corresponding calculated value, and $n = 60$ the total number of data we have considered (see the table in the Supplemental Material [79]). This analysis is analogous to the one reported in Fig. 1 of Ref. [16], where the authors evidenced the need to introduce a quenching factor $q \approx 0.74$ of the axial coupling constant g_A to reproduce at best GT data of nuclei in the $0f1p$ region with SM eigenfunctions obtained by diagonalizing the KB3 SM Hamiltonian [86].

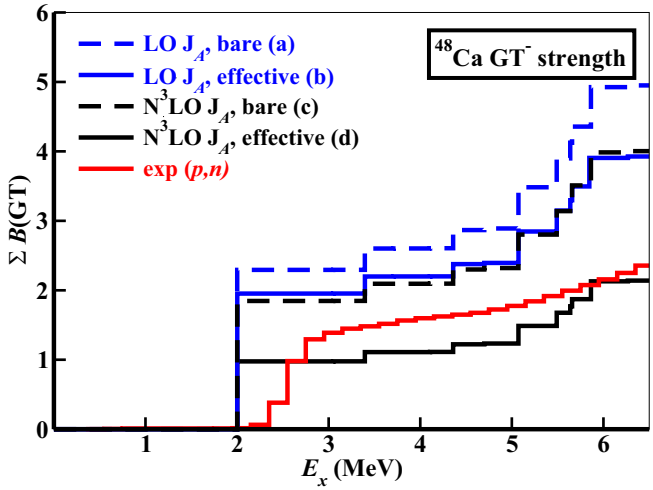

FIG. 11. Running sums of the ^{48}Ca B(GT) strengths as a function of the excitation energy E_x up to 6.5 MeV (see text for details).

From the inspection of Fig. 10, the best overall reproduction of the data is obtained by carrying out calculations with the effective operator (d), and the values of σ obtained with the operators (b) and (c) show that for the $0f1p$ shell the improvements we obtain with respect to the results with the bare operator (a) can be equally ascribed to the renormalization of the GT operator by way of the ChPT expansion of $\mathbf{J}_A$, as well as to the derivation of SM effective operators which account for the configurations outside the model space (see Sec. II C).

Another quantity that is indirectly related to the GT decay operator, and that is worth studying, is the GT strength distribution:

$$B(\mathrm{GT}) = \frac{\left|\langle \Phi_f || \mathbf{J}_A/g_A || \Phi_i \rangle\right|^2}{2J_i + 1}, \tag{22}$$

where indices i, f refer to the parent and daughter nuclei, respectively.

They are obtained from charge-exchange reactions, and can be extracted from the GT component of the cross section at zero degrees, following the standard approach in the distorted-wave Born approximation (DWBA):

$$\frac{d\sigma^{\mathrm{GT}}(0^\circ)}{d\Omega} = \left(\frac{\mu}{\pi\hbar^2}\right)^2 \frac{k_f}{k_i} N_D^{\sigma\tau} |J_{\sigma\tau}|^2 B(\mathrm{GT}),$$

where $N_D^{\sigma\tau}$ is the distortion factor, $|J_{\sigma\tau}|$ is the volume integral of the effective NN interaction, k_i and k_f are the initial and final momenta, respectively, and μ is the reduced mass (see the formula and description in Refs. [87,88]). This means that the values of experimental GT strengths are somehow model dependent.

In Fig. 11, the calculated running sums of the GT$^-$ strengths [ΣB(GT)] for ^{48}Ca are shown as a function of the excitation energy up to 6.5 MeV, and compared with the data reported with a red line [89]. The results obtained with the bare operator (a) are drawn with a blue dashed line, and those obtained employing the effective GT operator at LO of the chiral perturbative expansion of $\mathbf{J}_A$ (II) are plotted with a solid blue line. The results with the operators (c) and (d), namely with a bare and effective axial current $\mathbf{J}_A$ expanded up to N^{3}LO, are drawn with dashed and solid black lines, respectively.

It can be seen that the distributions obtained using the (b) and (c) operators nearly overlap, confirming that the contributions to the renormalization of the GT operator due to the ChPT expansion of $\mathbf{J}_A$ and to the derivation of a SM effective decay operator have the same effect in this mass region.

The combination of both effects, which operator (d) accounts for, results in a good reproduction of the values extracted from data. It should be pointed out that the theoretical total GT$^-$ strengths are 24.0, 17.5, 20.9, and 11.2 with operators (a)–(d), respectively, which should be compared with an experimental one that is 15.3 ± 2.2 and includes a possible contribution from an isovector spin monopole (IVSM) component [89].

TABLE II. Experimental [90,91] and calculated $M^{2\nu}$'s (in MeV^{-1}) for ^{48}Ca $2\nu\beta\beta$ decay.

$J_i^\pi \to J_f^\pi$	(a)	(b)	(c)	(d)	Expt.
			^{48}Ca $\to$ ^{48}Ti		
$0_1^+ \to 0_1^+$	0.057	0.048	0.033	0.019	0.042 ± 0.004
$0_1^+ \to 2_1^+$	0.131	0.102	0.097	0.058	$\leqslant 0.023$
$0_1^+ \to 0_2^+$	0.102	0.086	0.073	0.040	$\leqslant 2.72$

In Table II we report the observed and calculated values of the $M^{2\nu}$'s for the $2\nu\beta\beta$ decay from ^{48}Ca ground state into ^{48}Ti yrast $J^\pi = 0^+, 2^+$ and yrare $J^\pi = 0^+$ states; only for $0_1^+ \to 0_1^+$ there is a measured value [90], while for the other transitions there are experimental upper bounds [91]. We point out that, with respect to the expression in Eq. (19), results are expressed in g_A^2 units.

We note that both the experimental and calculated values of $M^{2\nu}$ are rather small, compared with those corresponding to the $2\nu\beta\beta$ decay of other nuclides (see Ref. [90] for a recent review of current data). Regarding our calculated $M^{2\nu}$'s in Table II, we have to underline that their reduced magnitude is mainly related to the fact that there is some cancellation between the different terms appearing in the sum in Eq. (19).

We may observe that, for the decay between the ground states of ^{48}Ca and ^{48}Ti, the $M^{2\nu}$ obtained with the bare operator (a) slightly overestimates the experimental one, and it is three times larger than the one obtained with the effective operator (d), which accounts for the ChPT expansion of $\mathbf{J}_A$ as well as the renormalization due to the configurations outside the chosen $0f1p$ model space. This corresponds to a quenching factor $q \approx 0.6$, which is slightly smaller of the empirical value $q = 0.7$ commonly considered in most of calculations that resort to a truncation of the nuclear degrees of freedom [9,16].

Regarding the role of the two-body electroweak currents, it is worth noting that the value of the calculated $M^{2\nu}$'s with SM effective operator (d) when compared with the experimental one is very satisfactory and similar to the result $M^{2\nu} = 0.026\mathrm{MeV}^{-1}$ we obtained by deriving H_{eff} and Θ_{eff} from the CD-Bonn potential, renormalized by way of the $V_{\mathrm{low}\text{-}k}$ procedure [10].

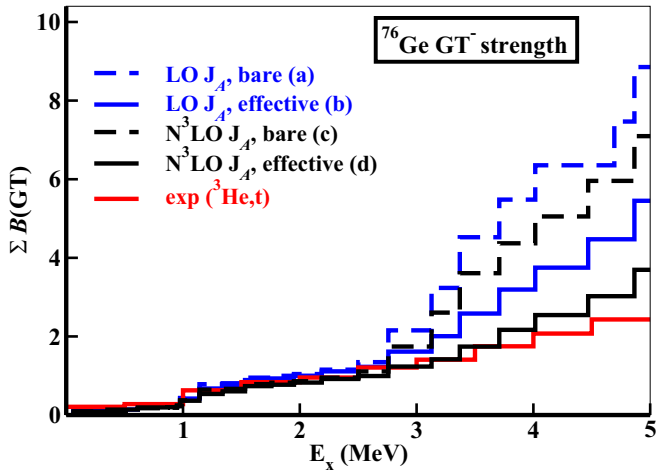

FIG. 12. Running sums of the ^{76}Ge B(GT) strengths as a function of the excitation energy E_x up to 5 MeV.

Now, we focus our attention on $0\nu\beta\beta$-decay candidates which belong to the $0f_{5/2}1p0g_{9/2}$ shell, namely ^{76}Ge and ^{82}Se.

For the calculation of GT-decay properties within such a model space, we expect that the role of the SM effective operator increases, since it is well known [19] that spin- and spin-isospin-dependent operators need larger renormalizations if some of the orbitals belonging to the model space—specifically $0f_{5/2}$ and $0g_{9/2}$—lack their spin-orbit counterpart.

We start from the comparison between the experimental [92,93] and the calculated running sums of the GT$^-$ strengths for ^{76}Ge and ^{82}Se, that are reported in Figs. 12 and 13, respectively. The same labeling as in Fig. 11 is used, namely the blue dashed line represents the calculated values with the bare operator (a), those obtained with operator (b) are shown with a solid blue line. The results with the operators (c) and (d) are plotted with dashed and solid black lines, respectively.

As can be observed in both Figs. 12 and 13, especially for higher energies, only the inclusion of both many-body renormalizations and higher-order terms in the ChPT expansion

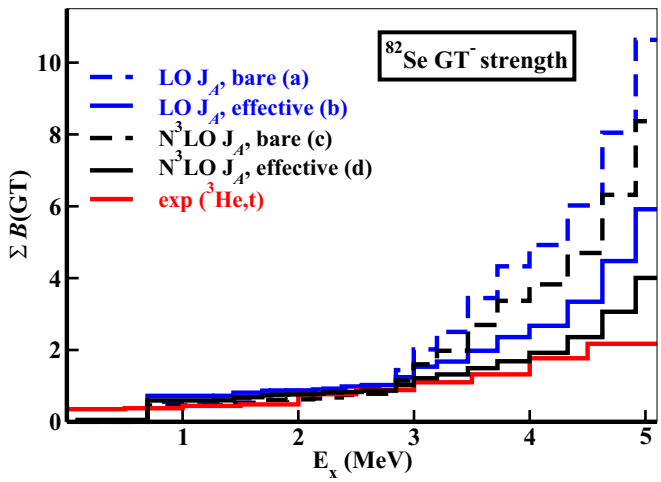

FIG. 13. Same as in Fig. 12, but for ^{82}Se.

TABLE III. Experimental [90,91] and calculated $M^{2\nu}$'s (in MeV^{-1}) for ^{76}Ge and ^{82}Se $2\nu\beta\beta$ decay.

$J_i^\pi \to J_f^\pi$	(a)	(b)	(c)	(d)	Expt.
			^{76}Ge $\to$ ^{76}Se		
$0_1^+ \to 0_1^+$	0.211	0.153	0.160	0.118	0.129 ± 0.004
$0_1^+ \to 2_1^+$	0.023	0.042	0.025	0.048	$\leqslant 0.035$
$0_1^+ \to 0_2^+$	0.009	0.086	0.016	0.063	$\leqslant 0.089$
			^{82}Se $\to$ ^{82}Kr		
$0_1^+ \to 0_1^+$	0.173	0.123	0.136	0.095	0.103 ± 0.001
$0_1^+ \to 2_1^+$	0.003	0.006	0.008	0.033	$\leqslant 0.020$
$0_1^+ \to 0_2^+$	0.018	0.007	0.013	0.007	$\leqslant 0.052$

can provide a quite good reproduction of the observed GT-strength distribution. The theoretical total GT$^-$ strengths are 15.8, 10.8, 12.8, and 7.4 with operators (a)–(d), respectively, for ^{76}Ge and 19.0, 11.4, 14.9, and 7.5 for ^{82}Se. At present, there are no available data for these quantities.

Before closing the discussion about the GT-strength distributions, it is worth emphasizing that, starting from an excitation energy of ≈4 MeV, the experimental distributions are affected by the underlying contributions arising from the rather structureless tail of the Gamow-Teller resonance (GTR). Actually, broad GTRs are observed around $E_x = 11$ and 12.1 MeV in ^{76}Ge and ^{82}Se, respectively, and their contribution to the total GT strength is not easy to evaluate quantitatively [92,93].

The central role of two-body electroweak currents shows up also in the comparison among the calculated $M^{2\nu}$'s for the $2\nu\beta\beta$ decay of the ^{76}Ge ground state into the ^{76}Se one, as well as for the same $2\nu\beta\beta$ decay of ^{82}Se into ^{82}Kr, whose values are reported in Table III.

The comparison of experimental $0_1^+ \to 0_1^+$ $M^{2\nu}$'s with those calculated by employing SM effective operators (d) is very satisfactory. The theoretical values are similar to the ones we have obtained by deriving $H_{\rm eff}$ and $\Theta_{\rm eff}$ from the CD-Bonn potential, renormalized by way of the $V_{\text{low-}k}$ procedure [10]. In this connection, it is worth noting that the renormalization of the one-body GT operator $\boldsymbol{\sigma\tau}$ due to the use of a truncated model space is smaller for the $H_{\rm eff}$'s employed in the present paper than the one obtained using the $H_{\rm eff}$'s derived in Ref. [10].

The calculated values of $0_1^+ \to 2_1^+, 0_2^+$ $M^{2\nu}$'s are much smaller than the ones involving the transitions between the ground states, despite being characterized by smaller Q values. This happens because the contributions corresponding to the different intermediate states in Eq. (19) tend to cancel each other for such decay branches, while for the decay to the ground states of ^{76}Se and ^{82}Kr they are mostly coherent in sign.

IV. SUMMARY AND OUTLOOK

In this work we have studied for the first time the impact of two-body electroweak currents, derived with chiral perturbation theory, on the perturbative renormalization of the shell-model GT-decay effective operator.

To this end, the electroweak currents have been calculated by way of a perturbative expansion up to next-to-next-to-next-to-leading order in chiral perturbation theory, that provides both single- and two-body components; then the SM effective GT operators have been derived by way of many-body perturbation theory. Using such a framework, the SM effective Hamiltonians have been constructed starting from chiral two- and three-body forces—which share the same low-energy constants with the expansion of the electroweak currents—and then employing the so-called $\hat{Q}$-box-plus-folded-diagram method to derive the single-particle energies and two-body matrix elements of the residual Hamiltonian.

This study is a part of a project aiming to calculate reliable nuclear matrix elements of the $0\nu\beta\beta$ decay, therefore we have applied the present theoretical approach to nuclei of the $0f1p$ and $0f_{5/2}1p0g_{9/2}$ shells that are of experimental interest for the detection of such a rare process, namely ^{48}Ca, ^{76}Ge, and ^{82}Se.

The comparison of our results with experiment for a large set of observables related to the GT decay—especially the nuclear matrix elements of $2\nu\beta\beta$ decay—show that the chiral expansion of the electroweak currents and the many-body renormalizations, which account for the configurations outside the model space, share equal merit in providing a noteworthy reproduction of data. These results, together with a good reproduction of low-energy spectroscopic properties of the parent and granddaughter nuclei, should support the reliability of our future calculation of the nuclear matrix elements $M^{0\nu}$'s for $0\nu\beta\beta$ decay.

In fact the future development of our scientific project is to move towards a similar study that will involve heavier systems such as ^{100}Mo, that are more challenging from the point of view of a shell-model calculation, as well as the prediction of their $0\nu\beta\beta$ with nuclear matrix elements. In this way, we could also compare the results based on the ChPT expansion of nuclear Hamiltonians and electroweak currents with those we have previously obtained within the realistic shell model starting from the two-body CD-Bonn potential that was constructed by way of the meson-exchange theory [36].

Thus, our following work may also provide important information to narrow down the spread of the predicted $M^{0\nu}$'s obtained by way of different approaches.

ACKNOWLEDGMENTS

We thank T. Miyagi for helpful discussion on the inclusion of two-body currents using the shell-model code KSHELL. G.D.G. acknowledges support from the EU-FESR, PON Ricerca e Innovazione 2014–2020, DM 1062/2021. We acknowledge a CINECA award under the ISCRA initiative and under the INFN-CINECA agreement, for the availability of high performance computing resources and support. We acknowledge the support from the National Natural Science Foundation of China under Grants No. 11835001, No. 11921006, and No. 12035001.

[1] P. Pirinen and J. Suhonen, Phys. Rev. C **91**, 054309 (2015).
[2] B. A. Brown, D. L. Fang, and M. Horoi, Phys. Rev. C **92**, 041301(R) (2015).
[3] F. Šimkovic, R. Dvornický, D. Štefánik, and A. Faessler, Phys. Rev. C **97**, 034315 (2018).
[4] D. S. Delion and J. Suhonen, Phys. Rev. C **95**, 034330 (2017).
[5] J. Suhonen, Phys. Rev. C **96**, 055501 (2017).
[6] L. Coraggio, L. De Angelis, T. Fukui, A. Gargano, and N. Itaco, Phys. Rev. C **95**, 064324 (2017).
[7] E. A. Coello Pérez, J. Menéndez, and A. Schwenk, Phys. Rev. C **98**, 045501 (2018).
[8] E. A. C. Pérez, J. Menéndez, and A. Schwenk, Phys. Lett. B **797**, 134885 (2019).
[9] J. Suhonen and J. Kostensalo, Front. Phys. **7**, 29 (2019).
[10] L. Coraggio, L. De Angelis, T. Fukui, A. Gargano, N. Itaco, and F. Nowacki, Phys. Rev. C **100**, 014316 (2019).
[11] F. F. Deppisch, L. Graf, and F. Šimkovic, Phys. Rev. Lett. **125**, 171801 (2020).
[12] D. Gambacurta, M. Grasso, and J. Engel, Phys. Rev. Lett. **125**, 212501 (2020).
[13] L. Coraggio, N. Itaco, G. De Gregorio, A. Gargano, R. Mancino, and F. Nowacki, Phys. Rev. C **105**, 034312 (2022).
[14] J. Suhonen and O. Civitarese, Phys. Lett. B **725**, 153 (2013).
[15] H. Ejiri, Nucl. Phys. A **396**, 181 (1983).
[16] G. Martínez-Pinedo, A. Poves, E. Caurier, and A. P. Zuker, Phys. Rev. C **53**, R2602 (1996).
[17] J. Barea, J. Kotila, and F. Iachello, Phys. Rev. C **91**, 034304 (2015).
[18] H. Hyuga and A. Arima, J. Phys. Soc. Jpn. Suppl. **34**, 538 (1973).
[19] I. S. Towner, Phys. Rep. **155**, 263 (1987).
[20] J. Kotila and F. Iachello, Phys. Rev. C **85**, 034316 (2012).
[21] K. Shimizu, M. Ichimura, and A. Arima, Nucl. Phys. A **226**, 282 (1974).
[22] I. S. Towner and K. F. C. Khanna, Nucl. Phys. A **399**, 334 (1983).
[23] A. Arima, K. Shimizu, and W. Bentz, Adv. Nucl. Phys. **18**, 1 (2003).
[24] T. T. S. Kuo and G. E. Brown, Nucl. Phys. **85**, 40 (1966).
[25] T. T. S. Kuo, S. Y. Lee, and K. F. Ratcliff, Nucl. Phys. A **176**, 65 (1971).
[26] T. T. S. Kuo and E. Osnes, *Folded-Diagram Theory of the Effective Interaction in Nuclei, Atoms and Molecules*, Lecture Notes in Physics (Springer-Verlag, Berlin, 1990), Vol. 364.
[27] M. Lacombe, B. Loiseau, J. M. Richard, R. Vinh Mau, J. Côtè, P. Pirés, and R. de Tourreil, Phys. Rev. C **21**, 861 (1980).
[28] R. V. Reid, Ann. Phys. (NY) **50**, 411 (1968).
[29] H. F. Wu, H. Q. Song, T. T. S. Kuo, W. K. Cheng, and D. Strottman, Phys. Lett. B **162**, 227 (1985).
[30] H. Q. Song, H. F. Wu, and T. T. S. Kuo, Phys. Lett. B **259**, 229 (1991).
[31] A. Baroni, L. Girlanda, A. Kievsky, L. E. Marcucci, R. Schiavilla, and M. Viviani, Phys. Rev. C **94**, 024003 (2016).
[32] T. T. S. Kuo, J. Shurpin, K. C. Tam, E. Osnes, and P. J. Ellis, Ann. Phys. (NY) **132**, 237 (1981).
[33] K. Suzuki and R. Okamoto, Prog. Theor. Phys. **93**, 905 (1995).

[34] L. Coraggio, A. Covello, A. Gargano, N. Itaco, and T. T. S. Kuo, Ann. Phys. (NY) **327**, 2125 (2012).
[35] L. Coraggio, and N. Itaco, Front. Phys. **8**, 345 (2020).
[36] R. Machleidt, Phys. Rev. C **63**, 024001 (2001).
[37] S. Bogner, T. T. S. Kuo, L. Coraggio, A. Covello, and N. Itaco, Phys. Rev. C **65**, 051301(R) (2002).
[38] E. Epelbaum, H.-W. Hammer, and Ulf-G. Meißner, Rev. Mod. Phys. **81**, 1773 (2009).
[39] R. Machleidt and D. R. Entem, Phys. Rep. **503**, 1 (2011).
[40] T. S. Park, D. P. Min, and M. Rho, Phys. Rep. **233**, 341 (1993).
[41] S. Pastore, L. Girlanda, R. Schiavilla, M. Viviani, and R. B. Wiringa, Phys. Rev. C **80**, 034004 (2009).
[42] A. Baroni, L. Girlanda, S. Pastore, R. Schiavilla, and M. Viviani, Phys. Rev. C **93**, 015501 (2016).
[43] G. B. King, L. Andreoli, S. Pastore, M. Piarulli, R. Schiavilla, R. B. Wiringa, J. Carlson, and S. Gandolfi, Phys. Rev. C **102**, 025501 (2020).
[44] A. Baroni, G. B. King, and S. Pastore, Few-Body Syst. **62**, 114 (2021).
[45] A. Gnech, L. E. Marcucci, R. Schiavilla, and M. Viviani, Phys. Rev. C **104**, 035501 (2021).
[46] A. Gnech, and R. Schiavilla, Phys. Rev. C **106**, 044001 (2022).
[47] G. B. King, A. Baroni, V. Cirigliano, S. Gandolfi, L. Hayen, E. Mereghetti, S. Pastore, and M. Piarulli, Phys. Rev. C **107**, 015503 (2023).
[48] P. Gysbers, G. Hagen, J. D. Holt, G. R. Jansen, T. D. Morris, P. Navrátil, T. Papenbrock, S. Quaglioni, A. Schwenk, S. R. Stroberg *et al.*, Nat. Phys. **15**, 428 (2019).
[49] D. R. Entem and R. Machleidt, Phys. Rev. C **66**, 014002 (2002).
[50] P. Navrátil, V. G. Gueorguiev, J. P. Vary, W. E. Ormand, and A. Nogga, Phys. Rev. Lett. **99**, 042501 (2007).
[51] Y. Z. Ma, L. Coraggio, L. De Angelis, T. Fukui, A. Gargano, N. Itaco, and F. R. Xu, Phys. Rev. C **100**, 034324 (2019).
[52] U. van Kolck, Prog. Part. Nucl. Phys. **43**, 337 (1999).
[53] S. Weinberg, Physica A **96**, 327 (1979).
[54] D. R. Entem and R. Machleidt, Phys. Rev. C **68**, 041001(R) (2003).
[55] S. Weinberg, Phys. Lett. B **295**, 114 (1992).
[56] U. van Kolck, Phys. Rev. C **49**, 2932 (1994).
[57] T. Fukui, L. De Angelis, Y. Z. Ma, L. Coraggio, A. Gargano, N. Itaco, and F. R. Xu, Phys. Rev. C **98**, 044305 (2018).
[58] L. Coraggio, G. De Gregorio, A. Gargano, N. Itaco, T. Fukui, Y. Z. Ma, and F. R. Xu, Phys. Rev. C **102**, 054326 (2020).
[59] L. Coraggio, G. De Gregorio, A. Gargano, N. Itaco, T. Fukui, Y. Z. Ma, and F. R. Xu, Phys. Rev. C **104**, 054304 (2021).
[60] S. Kölling, E. Epelbaum, H. Krebs, and U. G. Meißner, Phys. Rev. C **80**, 045502 (2009).
[61] H. Krebs, E. Epelbaum, and U. G. Meißner, Ann. Phys. **378**, 317 (2017).
[62] H. Krebs, Eur. Phys. J. A **56**, 234 (2020).
[63] J. Menéndez, D. Gazit, and A. Schwenk, Phys. Rev. Lett. **107**, 062501 (2011).
[64] M. Hjorth-Jensen, T. T. S. Kuo, and E. Osnes, Phys. Rep. **261**, 125 (1995).
[65] K. Suzuki and S. Y. Lee, Prog. Theor. Phys. **64**, 2091 (1980).
[66] K. Suzuki, R. Okamoto, H. Kumagai, and S. Fujii, Phys. Rev. C **83**, 024304 (2011).
[67] *An Advanced Course in Computational Nuclear Physics*, edited by M. Hjorth-Jensen, M. P. Lombardo, and U. van Kolck, Lecture Notes in Physics (Springer, Berlin, 2017), Vol. 936.
[68] J. D. Holt, J. Menéndez, J. Simonis, and A. Schwenk, Phys. Rev. C **90**, 024312 (2014).
[69] N. Shimizu, T. Mizusaki, Y. Utsuno, and Y. Tsunoda, Comput. Phys. Commun. **244**, 372 (2019).
[70] A. Polls, H. Müther, A. Faessler, T. T. S. Kuo, and E. Osnes, Nucl. Phys. A **401**, 124 (1983).
[71] G. Audi, A. H. Wapstra, and C. Thibault, Nucl. Phys. A **729**, 337 (2003).
[72] J. Blomqvist and A. Molinari, Nucl. Phys. A **106**, 545 (1968).
[73] L. Coraggio, L. De Angelis, T. Fukui, A. Gargano, and N. Itaco, J. Phys.: Conf. Ser. **1056**, 012012 (2018).
[74] L. Coraggio, A. Gargano, N. Itaco, R. Mancino, and F. Nowacki, Phys. Rev. C **101**, 044315 (2020).
[75] W. C. Haxton and G. J. Stephenson Jr., Prog. Part. Nucl. Phys. **12**, 409 (1984).
[76] S. R. Elliott and P. Vogel, Annu. Rev. Nucl. Part. Sci. **52**, 115 (2002).
[77] E. Caurier, G. Martínez-Pinedo, F. Nowacki, A. Poves, and A. P. Zuker, Rev. Mod. Phys. **77**, 427 (2005).
[78] J. Kotila and F. Iachello, Phys. Rev. C **87**, 024313 (2013).
[79] See Supplemental Material at http://link.aps.org/supplemental/10.1103/PhysRevC.109.014301 for the list of SP energies and two-body matrix elements of the shell-model Hamiltonian $H_{\rm eff}$, derived for one- and two-valence-nucleon systems in the $0f_{5/2}1p0g_{9/2}$ model space, and for the list of the 60 matrix elements of the GT decay of $0f1p$-shell nuclei.
[80] Data extracted using the NNDC On-line Data Service from the ENSDF database, https://www.nndc.bnl.gov/ensdf.
[81] L. Coraggio, A. Covello, A. Gargano, and N. Itaco, Phys. Rev. C **89**, 024319 (2014).
[82] Y. Utsuno, T. Otsuka, T. Mizusaki, and M. Honma, Phys. Rev. C **60**, 054315 (1999).
[83] T. Otsuka, A. Gade, O. Sorlin, T. Suzuki, and Y. Utsuno, Rev. Mod. Phys. **92**, 015002 (2020).
[84] Y. Toh, C. J. Chiara, E. A. McCutchan, W. B. Walters, R. V. F. Janssens, M. P. Carpenter, S. Zhu, R. Broda, B. Fornal, B. P. Kay, F. G. Kondev, W. Krolas, T. Lauritsen, C. J. Lister, T. Pawlat, D. Seweryniak, I. Stefanescu, N. J. Stone, J. Wrzesinski, K. Higashiyama, and N. Yoshinaga, Phys. Rev. C **87**, 041304(R) (2013).
[85] D. Rhodes, B. A. Brown, A. Gade, S. Biswas, A. Chester, P. Farris, J. Henderson, A. Hill, J. Li, F. Nowacki *et al.*, Phys. Rev. C **105**, 024325 (2022).
[86] A. Poves and A. Zuker, Phys. Rep. **70**, 235 (1981).
[87] P. Puppe, A. Lennarz, T. Adachi, H. Akimune, H. Ejiri, D. Frekers, H. Fujita, Y. Fujita, M. Fujiwara, E. Ganioğlu *et al.*, Phys. Rev. C **86**, 044603 (2012).
[88] D. Frekers, P. Puppe, J. H. Thies, and H. Ejiri, Nucl. Phys. A **916**, 219 (2013).
[89] K. Yako, M. Sasano, K. Miki, H. Sakai, M. Dozono, D. Frekers, M. B. Greenfield, K. Hatanaka, E. Ihara, M. Kato *et al.*, Phys. Rev. Lett. **103**, 012503 (2009).
[90] A. Barabash, Universe **6**, 159 (2020).
[91] P. Belli, R. Bernabei, F. Cappella, V. Caracciolo, R. Cerulli, A. Incicchitti, and V. Merlo, Universe **6**, 239 (2020).
[92] J. H. Thies, D. Frekers, T. Adachi, M. Dozono, H. Ejiri, H. Fujita, Y. Fujita, M. Fujiwara, E.-W. Grewe, K. Hatanaka *et al.*, Phys. Rev. C **86**, 014304 (2012).
[93] D. Frekers, M. Alanssari, T. Adachi, B. T. Cleveland, M. Dozono, H. Ejiri, S. R. Elliott, H. Fujita, Y. Fujita, M. Fujiwara *et al.*, Phys. Rev. C **94**, 014614 (2016).